Turkish Journal of Electrical Engineering & Computer Sciences

http://journals.tubitak.gov.tr/elektrik/

Research Article

Turk J Elec Eng & Comp Sci
(2016) 24: 427 – 434

doi:10.3906/elk-1305-70

Extracting the region of interest from MFL signals

Ali SADR*, Raziyeh Sadat OKHOVAT
Department of Electrical Engineering, Iran University of Science and Technology, Tehran, Iran

Received: 08.05.2013 • **Accepted/Published Online:** 21.11.2013 • **Final Version:** 05.02.2016

Abstract: In this paper, we study the magnetic flux leakage (MFL) signals for detection of defects in ferromagnetic materials. MFL signals consist of a background that is not constant and is combined with noise. Since there are slight variations because of noise, any large distortion shows a defect. Here the estimation of the background and then the determination of a threshold to distinguish defects from noise have been used for locating defects. In this method, precise evaluation of these two parameters has a vital role on the defect detection. The concept of histograms has been employed for eliminating the effect of defects in computing background signal. Results show that this algorithm is fast enough and yields detection of more defects that have lower amplitude. In the next step, an appropriate value for the threshold is determined by considering a trade-off between defect detection rate and noise separation rate.

Key words: Nondestructive test, magnetic flux leakage signals, defect detection, histogram, background signal, threshold

1. Introduction

The magnetic flux leakage (MFL) technique is one of the nondestructive test (NDT) methods employed for detection of defects in ferromagnetic structures like pipelines, rail tracks, and bridges [1–4]. We restrict our studies to the signals that are obtained from an intelligent pipeline inspection gauge used for inspection of gas and oil pipelines. In this technique, the pipeline's walls are saturated by magnetic flux. Most of the defects such as gouges, corrosion, dents, and cracking lead to the flux leakage in the air and therefore the amplitude of MFL signals will be increased. Some other defects such as clamp and weld cause MFL signals to decrease.

MFL data are usually contaminated by various sources of noise including sensor lift-off variations, seamless pipe noise (SPN), and variations in the steel magnetic properties due to alloying elements and system noise. Some of them like SPN can completely mask MFL signals from certain types of defects such as shallow corrosion and mechanical damage. A new method was proposed by Afzal and Udpa [5] that applies the time domain adaptive filter to remove the SPN noise. Four years later Han and Que [6] presented a new denoising approach based on the wavelet domain adaptive FIR filter.

On the other hand, the width and height of distortion in MFL signals can be exploited for the determination of the defect size [7]. Naemi et al. [8] and Katoh et al. [9] used 2D finite element method modeling to generate MFL signals from defects of various shapes. All these theoretical calculations agree well with the experimental results from defects with simple shapes. However, the traditional measurement of 2D magnetic fields cannot accurately characterize natural defects. Regarding this specific subject, Zuoying et al. [10], Li et al. [11], and Amineh et al. [12,13] conducted the measurement of 3D magnetic fields for better characterization.

*Correspondence: sadr@iust.ac.ir

Although the effect of stresses on flux leakage components is ignored in many cases, they have a vital role on MFL signal increase. Babbar et al. [14] and Wilson et al. [15] considered that MFL signals are affected not only by the geometry of the defect, but also by the presence of stresses. They scaled various stresses to make the MFL signals stress-independent.

The most important key in the above-mentioned signal processing methods is finding the region of interest (ROI) that includes the defects. Carvalho et al. [16] realized the location of defects by using neural networks. However, the large extent of the calculations is made by this procedure. In the present work, the histogram has been employed for background estimation. Furthermore, an appropriate threshold is exploited to distinguish defects from noise.

2. Methodology

In the MFL technique, a pipeline's walls are saturated by magnetic flux. If a defect causes an air gap in the specimen, the cross-sectional area of the pipeline decreases. Therefore, the magnetic flux lines cannot pass through the pipeline and leak outside. Figure 1 shows that the magnetic flux lines bulge outward. This is known as the fringing of the flux.

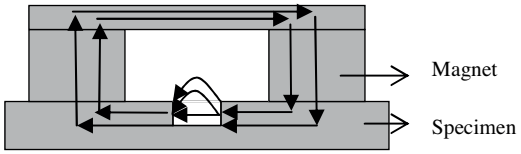

Figure 1. Creating magnetic flux by a permanent magnet.

2.1. Background estimation

Since the background of MFL signals is not constant and is combined with noise, there is not an exact value for it, and it is necessary to estimate it precisely. Averaging is a usual way for computing background. However, in this method, the amplitude of defects affects the calculation. In the case of most defects like gouges, corrosion, dents, and cracks, the background would be estimated as being more than the real value and as a result, some defects are not recognized. In other cases like clamping and welding, the background would be calculated as being less than the real value, and therefore noise may be considered as a defect.

The concept of histograms can be employed for canceling the effect of the defect in background estimation. In this way, peak location of the histogram shows the amplitude that occurs most of the time. On the other hand, as a result of large differences between background and signal amplitude in the defect location, they can be distinguished by the histogram. According to the previous discussion, background is computed by averaging of the amplitude around the histogram peak.

$$\text{background} = \frac{\sum_{i=L_{\min}}^{L_{\max}} (i \times \text{histogram}(i))}{\sum_{i=L_{\min}}^{L_{\max}} \text{histogram}(i)} \tag{1}$$

$L_{\min}$ and $L_{\max}$ are located on the horizontal axis, before and after the peak. Since the histogram peak of a noisy signal is not completely separated from nearby parts, $L_{\min}$ and $L_{\max}$ are selected so that the amplitude of the histogram in these two limits satisfies the conditions in Eq. (2). It is clear that α in Eq. (2) should be

less than one. Here we select a value of 0.1 to consider the possible boundary around the peak location of the histogram.

$$\begin{cases} histogram(L_{\min}) \leq \alpha \times peak \quad value \\ histogram(L_{\max}) \leq \alpha \times peak \quad value \end{cases} \tag{2}$$

In this approach, there is one parameter that should be chosen in a right way, and that is the length of the signal. If a small part of the original signal is considered and there is a defect in that part, the peak of the histogram occurs in the amplitude of the defect and therefore that defect will not be detectable. In contrast, there is not an upper limit for this parameter, and therefore it should be chosen large enough. In our signals that are obtained from a real pipeline and are provided by a petroleum company, defects are extracted from up to 100 samples. Therefore, it is suitable to consider the length of the signal as being more than 4–5 times bigger. For example, here 800 samples are considered for each process.

Figure 2 shows an example of a signal corresponding to a corrosion defect. Figure 3 depicts the histogram of the MFL signal shown in Figure 2. In accordance with Figure 3, the peak occurs approximately at the value of 50, and there is a distinctive part that contains the higher amplitude of the signal in the defect location. The background signal is calculated by averaging of the amplitude around the histogram peak. The result is equal to 48.62, as confirmed by Figure 2.

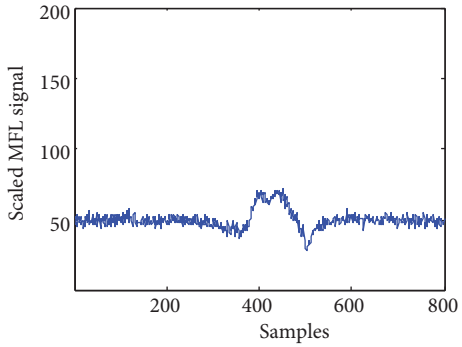

Figure 2. MFL signal for corrosion defect in pipeline.

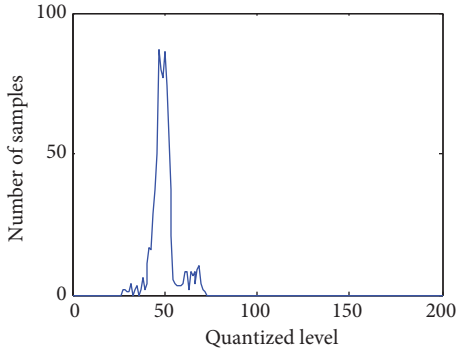

Figure 3. Histogram of MFL signal shown in Figure 2.

The histogram of Figure 4 is shown in Figure 5, and it consists of three separate parts. The first part is before the peak and includes points with lower amplitude. The second part is around the peak, and the third contains points with higher amplitude. According to the previous discussions, the background is computed by averaging of the second part of the histogram. Therefore neither lower nor higher amplitude affects the averaging. The result is equal to 49.74, as confirmed by Figure 4.

2.2. Threshold determination

Precision in extracting ROIs from MFL signals depends not only on the precise estimation of the background, but also on the legitimate value for the threshold. This parameter is a boundary limit to distinguish defect from noise. For choosing an appropriate value for the threshold, the relation between defect sizes and the magnetic flux leakage is studied. It is assumed that the pipeline's walls have been saturated by the permanent magnets. Therefore, the total magnetic flux in the pipeline is given by Eq. (3):

$$\varphi_t = B_s \times S \tag{3}$$

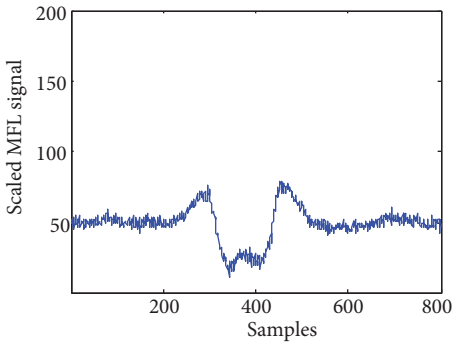

Figure 4. MFL signal for the placement of a clamp in the pipeline.

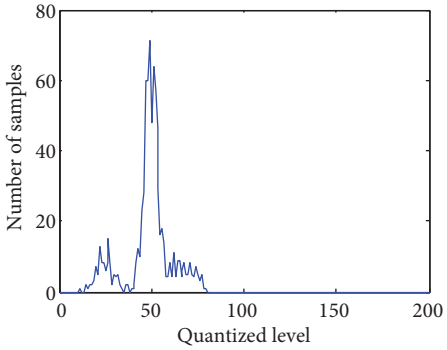

Figure 5. Histogram of MFL signal shown in Figure 4.

where B_s is the flux density of saturation and S is the cross-sectional area of the pipeline given by the following equation:

$$S = D \times W \tag{4}$$

where D and W are depth and width of the pipeline shown in Figure 6.

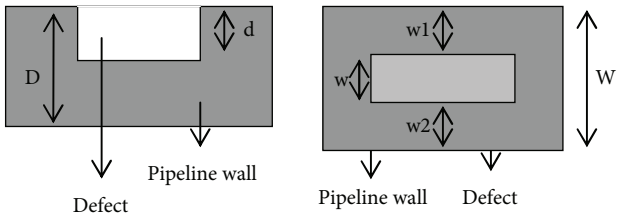

Figure 6. (a) Side view of defect in pipeline, (b) top view of defect in pipeline.

The effect of fringing is increasing the effective cross-sectional area of the air gap. The relation between flux in the air gap (φ_{ad}) and in the pipeline (φ_{pd}) at the defect location is given by Eq. (5):

$$\varphi_t = \varphi_{ad} + \varphi_{pd} \tag{5}$$

Since magnetic flux density in the pipeline is equal to B_s, this equation can be written in the following form:

$$B_s(D \times w) = \varphi_{ad} + B_s[(D - d) \times W] + B_s(d \times w1) + B_s(d \times w2) \tag{6}$$

Rearranging Eq. (6) yields:

$$\varphi_{ad} = B_s(d \times w) \tag{7}$$

As is seen from Eq. (7), magnetic flux leakage in the air gap is directly proportional to the width and depth of the defect. Therefore, shallow defects are detectable by choosing a small value for the threshold. However, they cannot be separated from noise and therefore noise may be considered as a defect in some places. On the other hand, a larger threshold results in detection of deeper defects, whereas noise is completely distinguished.

According to the previous discussion, there is a trade-off between defect detection rate and noise separation rate. Table 1 presents these two parameters at different values of the threshold for 340 noisy MFL signals provided by a petroleum company. The definition of threshold factor presented in this table is considered as:

$$\text{threshold} = (1 + \text{threshold} \quad \text{factor}) \ \times \text{background} \tag{8}$$

As is seen from Table 1, all defects are detectable by assigning 0.05 as the threshold factor. However, noise is considered as a defect in all 340 cases. On the other hand, the noise is completely distinguished from the defects by choosing a value of 0.45 for the threshold factor. However, 83 shallow defects cannot be detected.

Table 1. Defect detection rate and noise separation rate at different thresholds.

Threshold factor	Defect detection rate	Noise separation rate
0.05	100%	0%
0.1	100%	0%
0.15	98%	30%
0.2	97%	70%
0.25	94%	92%
0.3	68%	93%
0.35	43%	96%
0.4	32%	98%
0.45	24%	100%
0.5	10%	100%

The optimum value of the threshold is obtained by the intersection of two curves shown in Figure 7. According to this figure, the threshold factor is considered as:

$$\text{threshold} \quad \text{factor} = 0.25 \tag{9}$$

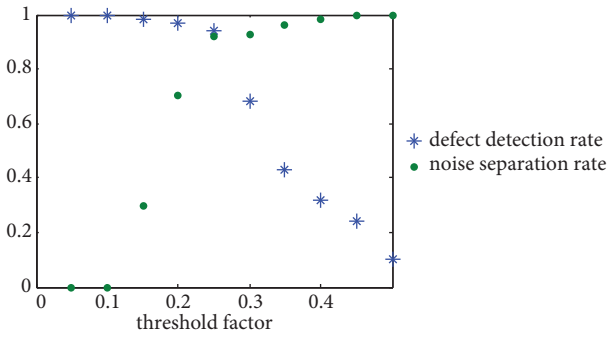

Figure 7. Defect detection rate and noise separation rate at different values of threshold.

2.3. Extracting the ROIs

Figures 8 and 9 depict the ROIs of the MFL signals shown in Figures 2 and 4, respectively. At first, the background is calculated by averaging of the amplitude around the histogram peak, and then the threshold value is obtained by assigning 0.25 to the threshold factor. Finally, for extracting the ROIs, the amplitude of signal is set to zero at points with lower amplitudes than the threshold and points with higher amplitudes than the threshold are considered as defects.

This simple algorithm cannot be exploited for the detection of ROIs in more complicated cases. Figures 10 and 11 show two examples of such cases. Figure 10 shows the MFL signal for a corrosion defect in the location of a clamp in the pipeline, whereas Figure 11 shows the MFL signal corresponding to the thickness increase in the pipeline. The thickness increase causes less flux to leak in the air and therefore the amplitude of the MFL signal will be decreased.

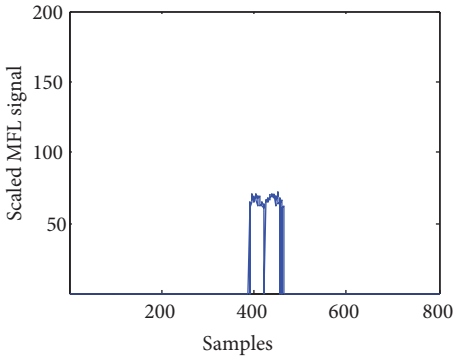

Figure 8. ROI of MFL signal shown in Figure 2.

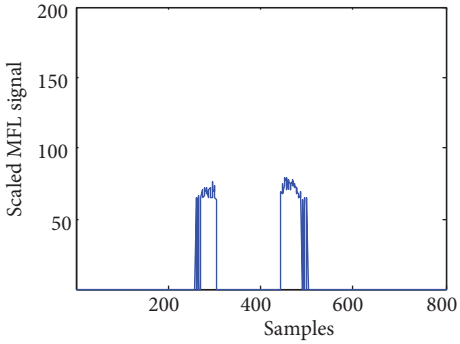

Figure 9. ROI of MFL signal shown in Figure 4.

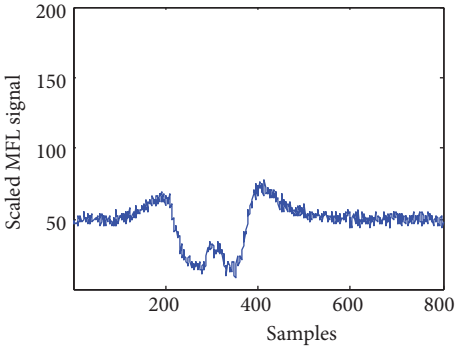

Figure 10. MFL signal for corrosion defect in location of a clamp.

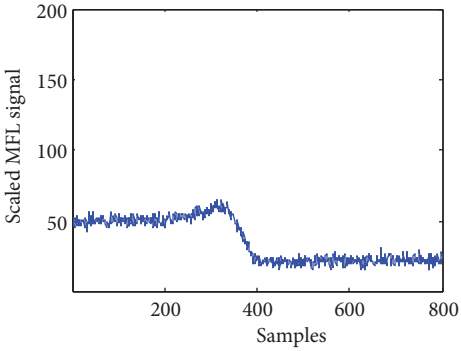

Figure 11. MFL signal for thickness increase in pipeline.

The histogram of Figure 10 is shown in Figure 12. Background and threshold values are equal to 51.2 and 64, respectively. If the amplitude of the signal is set to zero at points with lower amplitudes than the threshold, the region corresponding to a corrosion defect will be eliminated and therefore ROIs will not be detected completely.

The histogram of Figure 11 is shown in Figure 13. In accordance with Figure 13, the higher peak occurs at an amplitude around 20. The values of the background and threshold are equal to 19.3 and 24.1, respectively. If points with higher amplitudes than the threshold are considered as a defect, all parts of the pipeline with thinner thickness will be assumed as a defect.

For improving the defect detection rate in the mentioned cases, two boundary limits are assumed for a noisy background signal. These limits are determined in relation to the threshold factor:

$$L_{\max} = (1 + threshold \quad factor) \times background \tag{10}$$

$$L_{\min} = (1 - threshold \quad factor) \times background \tag{11}$$

For ROI detection, the amplitude of the signal at noisy background points is set to zero and the obtained signal is processed in a similar way again. Figures 14 and 15 depict the ROIs of MFL signals shown in Figures 10 and 11, respectively.

3. Results

Table 2 shows the results of the defect detection rate for two methods of computing background. In the first approach, the background is estimated by averaging of the signal. In this way, the amplitude of the signal

in the defect location affects the calculations and therefore the defect detection rate decreases. In the second method, the background is calculated by averaging of the amplitude around the histogram peak. Therefore, the background is estimated more precisely and the defect detection rate increases. The threshold factor is equal to 0.25 in both cases.

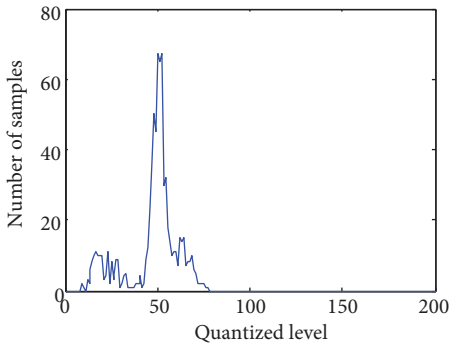

Figure 12. Histogram of MFL signal shown in Figure 10.

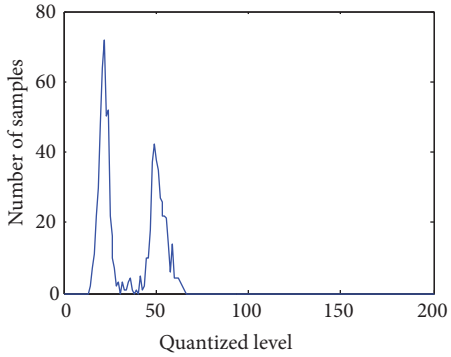

Figure 13. Histogram of MFL signal shown in Figure 11.

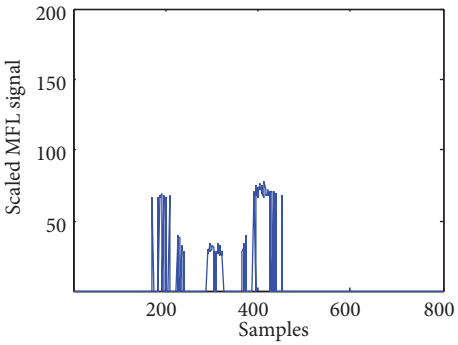

Figure 14. ROI of MFL signal shown in Figure 10.

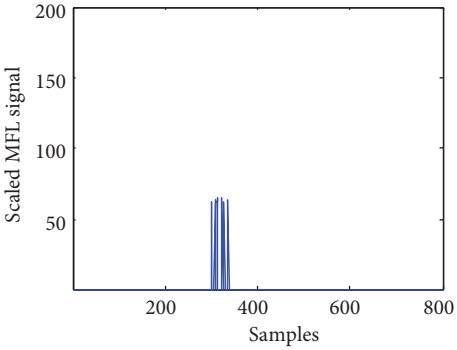

Figure 15. ROI of MFL signal shown in Figure 11.

Table 2. Defect detection rate by using two different methods for calculating background.

	Averaging of signal	Averaging of the amplitude around the histogram peak
Defect detection rate	91%	94%

4. Conclusion

One method for detection of ROIs includes background estimation and then determination of a threshold to distinguish defects from noise. In the present work, the concept of histograms has been employed for canceling the effect of defects in background estimation. This algorithm is fast enough and yields more precise values. Regarding an appropriate value for the threshold, the relation between magnetic flux leakage and defect sizes has been studied, and then the threshold has been chosen by considering a trade-off between defect detection rate and noise separation rate. In the next step, the noisy background is eliminated from MFL signals for detection of ROIs.

References

[1] Cheng SH, Wu X, Kang Y. Local area magnetization and inspection method for aerial pipelines. NDT&E Int 2005; 38: 448–452.

[2] Kosmas K, Sargentis CH, Tsamakis D, Hristoforou E. Non-destructive evaluation of magnetic metallic materials using Hall sensors. J Mater Process Tech 2005; 161: 359–362.

[3] Rainer P, Erhard A, Montag HJ, Thomas HM, Wüstenberg H. NDT techniques for railroad wheel and gauge corner inspection. NDT&E Int 2004; 37: 89–94.

[4] Ding J, Kang Y, Wu X. Tubing thread inspection by magnetic flux leakage. NDT&E Int 2006; 39: 53–56.

[5] Afzal M, Udpa S. Advanced signal processing of magnetic flux leakage data obtained from seamless gas pipeline. NDT&E Int 2002; 35: 449–457.

[6] Han W, Que P. A modified wavelet transform domain adaptive FIR filtering algorithm for removing the SPN in the MFL data. Measurement 2006; 39: 621–627.

[7] Bainton KF. Characterizing defects by determining magnetic leakage field. NDT&E Int 1977; 10: 253–257.

[8] Al-Naemi FI, Hall JP, Moses AJ. FEM modeling techniques of magnetic flux leakage-type NDT for ferromagnetic plate inspections. J Magn Magn Mater 2006; 304: 790–793.

[9] Katoh M, Masumoto N, Nishio K, Yamaguchi T. Modeling of the yoke-magnetization in MFL-testing by finite elements. NDT&E Int 2003; 36: 479–486.

[10] Zuoying H, Peiwen Q, Liang C. 3D FEM analysis in magnetic flux leakage method. NDT&E Int 2006, 39: 61–66.

[11] Li Y, Wilson J, Tian GY. Experiment and simulation study of 3D magnetic field sensing for magnetic flux leakage defect characterization. NDT&E Int 2007, 40: 179–184.

[12] Amineh RK, Nikolova NK, Reilly JP, Hare JR. Characterization of surface-breaking cracks using one tangential component of magnetic leakage field measurements. IEEE T Magn 2008, 44: 516–524.

[13] Amineh RK, Koziel S, Nikolova NK, Bandler JW, Reilly JP. A space mapping methodology for defect characterization from magnetic flux leakage measurements. IEEE T Magn 2008, 44: 2058–2065.

[14] Babbar V, Bryne J, Clapham L. Mechanical damage detection using magnetic flux leakage tools: modeling the effect of dent geometry and stresses. NDT&E Int 2005, 38: 471–477.

[15] Wilson J, Tian GY, Barrans S. Residual magnetic field sensing for stress measurement. Sensor Actuat A-Phys 2007, 135: 381–387.

[16] Carvalho AA, Rebello JMA, Sagrilo LVS, Camerini CS, Miranda IVJ. MFL signals and artificial neural networks applied to detection and classification of pipe weld defects. NDT&E Int 2006, 39: 661–667.